International Journal of Innovative
Computing, Information and Control
Volume **16**, Number **6**, December **2020**

 ISSN 1349-4198
pp. **1987–2005**

RESEARCH ON SYNCHRONOUS CONTROL STRATEGY OF ROBOT ARM BASED ON CROSS-COUPLING CONTROL

Xin Zhang[1,2], Wenru Lu[1], Miaohong Su[1] and Wenbo Xu[1]

[1]School of Automation and Electrical Engineering
[2]Gansu Provincial Engineering Research Center for Artificial Intelligence and Graphics and Image Processing
Lanzhou Jiaotong University
No. 88, Anning West Road, Anning District, Lanzhou 730070, P. R. China
18794206626@163.com

Received July 2020; revised November 2020

Abstract. *To reduce the contour errors from the coupling problem between the joints of the manipulators, we propose an integrated strategy combining the virtual spindle into the classical fractional order sliding mode cross-coupling control (FOSMC-CCC) strategy. Firstly, an iterative sliding mode control (ISMC) strategy is proposed to cope with single joint of manipulator, and the stability is proved by Lyapunov function and relative simulation. Secondly, on the basis of the single-joint control, FOSMC-CCC strategy is consequently proposed by using fractional order calculus, sliding mode control (SMC) and cross-coupling control (CCC) structure. Finally, the proposed method is verified by MATLAB/Simulink simulation. The simulation results show that compared with the traditional linear PD cross-coupling control (linear PD-CCC) strategy, the adjustment time is reduced by 0.14 s, 0.42 s and 0.35 s, and steady-state error is reduced by 0.0002 rad, 0.0004 rad and 0.0003 rad. Compared with nonlinear PD ring-coupling control (nonlinear PD-RCC) strategy, adjustment time is reduced by 0.12 s, 0.20 s and 0.16 s, and steady-state error is reduced by 0.0001 rad, 0.0002 rad and 0.0001 rad. The simulation results show that synchronous control accuracy of FOSMC-CCC strategy is better.*
Keywords: Cross-coupling control strategy, Fractional calculus, Iterative learning control, Manipulator control, Sliding mode control

1. **Introduction.** Since the 1960s, the rapid development of industrial robotic arms has become a core device in the field of automation. Nowadays, robotic arms have been widely used in industrial, agricultural and medical fields [1,2]. Many of these tasks require high-speed and high-precision trajectory tracking control, but the uncertainties, strong coupling, and time-varying characteristics of the robotic arm system make it difficult to establish its precise mathematical model, which brings certain obstacles to high-speed and high-precision trajectory tracking control. At the same time, the traditional manipulator control usually only considers the control of a single joint, but ignores the correlation between each joint. The tracking performance of single-joint control cannot guarantee the contour error control performance in multi-joint motion control, because when the synchronization between the joints is poor, the contour tracking accuracy of the system will decrease accordingly. Therefore, it is very important to study the synchronous control strategy between the joints of the mechanical arm.

For the problem of synchronous control, researchers have proposed many control structures, such as master-slave synchronous control [3,4], CCC [5-7], and RCC [8]. In [9], the CCC is proposed for the first time and is applied to traditional processing machine

DOI: 10.24507/ijicic.16.06.1987

tools, which can ensure the synchronization of each motor and reduce the system contour error. After that, many scholars carried out further research on multi-motor coordinated control. In [10], the global sliding mode control and CCC are combined to achieve synchronous control of precise positions of adjacent axes. In [11], an adjacent CCC strategy is proposed for the position synchronization control of multiple linear motors and achieves good synchronous control results. All of these methods can effectively improve the tracking performance of the system, but cannot effectively reduce the tracking error of a single axis. Therefore, it is necessary to improve the accuracy of the control system and reduce the contour error by combining independent position tracking control of each axis and the synchronization control between the axes.

Nowadays, scholars have proposed many algorithms about the control of the robot, such as traditional PID control algorithm [12], reverse step control algorithm [13], adaptive control algorithm [14], sliding mode control algorithm [15-17], neural network control algorithm and iterative learning control algorithm [18,19]. ILC does not rely on the precise mathematical model of the controlled object, and the control algorithm is simple [20-22]. SMC is robust to parameters and disturbances [23-27]. The combination of both can enhance the robustness of the system, suppress the chattering of system, and improve the control accuracy of robotic manipulator. Therefore, the robustness problem of ILC and the chattering phenomenon of SMC are solved [28-31]. In [32], an ISMC is designed, which utilizes the invariance of SMC to system parameters and external disturbances, and the advantage of ILC that does not depend on the precise mathematical model of the system, which improves the stability and dynamic response of the control system. In [33], the satellite attitude fault-tolerant control of external disturbances is studied by ILC and SMC.

The fractional order control system has been widely used in fractional order sliding mode control (FOSMC) and fractional order iterative learning control (FOILC) for its memory and heritability [34]. In [35], the robustness of PD-type FOILC algorithms is discussed. In [36], an effective FOSMC method is proposed, which verifies the good performance of the designed controller. However, few researchers have introduced fractional calculus into the control system of the manipulator, and the manipulator system has the characteristics of uncertainty, strong coupling and time-varying characteristics. Therefore, the parameters of the fractional calculus system can be adjusted to a large range and the system accuracy is high to control the complex manipulator system.

At the same time, the existing literature rarely studies the synchronization control of complex systems such as multi-joint manipulators, and the research on multi-joint manipulators only focuses on the synchronization performance between multiple joints, while ignoring the tracking effect of a single joint. Therefore, a control method combining single-joint tracking accuracy and multi-joint synchronization control accuracy is needed to improve the synchronization accuracy of the multi-joint robotic arm control system. Based on this, considering the coupling relationship between the joints of the robotic arm, in order to reduce the synchronization error between the joints and enhance the correlation between the joints, the FOSMC-CCC control strategy is proposed and verified via comparing with other control methods through simulation analysis. Mainly solve the following problems:

1) Improve the position tracking performance of the single joint of the robotic arm;

2) Enhance the robustness of the robotic arm control system and weaken the chattering phenomenon of the control system;

3) Reduce the contour error between multiple joints of the robotic arm and improve the synchronization accuracy of the control system.

In Section 2 the paper proposes the IMC position controller for the position tracking control of the single joint of the manipulator. Then in Sections 3 and 4, the FOSMC-CCC synchronization control strategy is proposed for the synchronization control research of the multi-joint manipulator, and the mathematical and simulation analysis respectively prove that the proposed synchronization control strategy has better synchronization accuracy in Section 5. Finally, in Section 6, the proposed control strategy is analyzed and summarized.

2. **Single Joint Tracking Control Strategy.** Manipulator control methods mainly include position control, continuous trajectory control, torque control and intelligent control. Among them, the continuous trajectory control method is to continuously control the posture of the robotic arm in space, requiring it to strictly follow a predetermined trajectory to move within a certain accuracy range, and the tracking effect is good, the movement is stable, and the task has been completed. Make each joint of the robot arm perform corresponding movement continuously and synchronously. The main technical index is to make the various joints of the robot arm follow the desired trajectory to track smoothly and accurately, usually in the robot arm used in arc welding, painting and inspection operations.

Caputo-type calculus is used in the paper, the definition of which is as follows [37]:

$$ {}_aD_t^{\beta} f(t) = \frac{1}{\Gamma(m-\alpha)} \int_a^t \frac{f^{(m)}(\tau)}{(t-\tau)^{\beta-m+1}} d\tau, \quad m-1 < \beta \leq m \tag{1} $$

where $\Gamma(\cdot)$ is the Gamma function. To simplify expression, use D^{β} instead of ${}_aD_t^{\beta}$.

The nominal model of n-joint manipulator is as follows:

$$ \boldsymbol{M}(\boldsymbol{q})\ddot{\boldsymbol{q}} + \boldsymbol{C}\left(\boldsymbol{q}, \dot{\boldsymbol{q}}\right)\dot{\boldsymbol{q}} + \boldsymbol{G}(\boldsymbol{q}) = \boldsymbol{u} + \boldsymbol{f}(t) \tag{2} $$

where $\boldsymbol{q} \in \boldsymbol{R}^n$ represents joint position of the robotic manipulator, $\dot{\boldsymbol{q}} \in \boldsymbol{R}^n$ and $\ddot{\boldsymbol{q}} \in \boldsymbol{R}^n$ represent velocity vector and acceleration vector respectively, $\boldsymbol{M}(\boldsymbol{q}) \in \boldsymbol{R}^{n\times n}$ represents inertia matrix, $\boldsymbol{C}\left(\boldsymbol{q}, \dot{\boldsymbol{q}}\right) \in \boldsymbol{R}^{n\times n}$ represents centrifugal force and Coriolis force matrix, $\boldsymbol{G}(\boldsymbol{q}) \in \boldsymbol{R}^n$ represents gravity term, $\boldsymbol{u} \in \boldsymbol{R}^n$ represents control torque, and $\boldsymbol{f}(t)$ represents uncertain disturbance term.

According to the dynamic model of the robotic manipulator, tracking error of each joint position can be defined as:

$$ \boldsymbol{e}(t) = \boldsymbol{q}_{\mathrm{d}}(t) - \boldsymbol{q}(t) \tag{3} $$

where $\boldsymbol{q}_{\mathrm{d}}(t)$ is the desired position trajectory of joint, and $\boldsymbol{q}(t)$ is the actual position trajectory of joint.

Take the second derivative of (3):

$$ \dot{\boldsymbol{e}} = \ddot{\boldsymbol{q}}_{\mathrm{d}} - \ddot{\boldsymbol{q}} \tag{4} $$

where $\ddot{\boldsymbol{q}}_{\mathrm{d}}$ is the expected acceleration of joint, and $\ddot{\boldsymbol{q}}$ is the actual acceleration of joint.

The sliding surface can be designed as:

$$ \boldsymbol{s} = \boldsymbol{c}\boldsymbol{e} + \dot{\boldsymbol{e}} \tag{5} $$

where $\boldsymbol{s}$ is the switching function, $\boldsymbol{c} = \mathrm{diag}(c_1, c_2, \ldots, c_n)$ is the compensation coefficient of sliding surface, $\boldsymbol{e}$ is the position error of joint, and $\dot{\boldsymbol{e}}$ is the speed error of joint.

Take the derivative of (5):

$$ \dot{\boldsymbol{s}} = \boldsymbol{c}\dot{\boldsymbol{e}} + \ddot{\boldsymbol{e}} \tag{6} $$

where $\ddot{\boldsymbol{e}}$ is the acceleration error of joint.

Substitute (2) and (4) into (6):

$$ \dot{\boldsymbol{s}} = \boldsymbol{c}\dot{\boldsymbol{e}} + \ddot{\boldsymbol{q}}_{\mathrm{d}} - \boldsymbol{M}^{-1}\left[\boldsymbol{u} + \boldsymbol{f}(t) - \boldsymbol{G} - \boldsymbol{C}\dot{\boldsymbol{q}}\right] \tag{7} $$

where $\boldsymbol{M}^{-1}$ is the inverse matrix of matrix $\boldsymbol{M}$.

The exponential reaching law is

$$\dot{\boldsymbol{s}} = -\boldsymbol{\lambda}\text{sign}(\boldsymbol{s}) - k\boldsymbol{s} \tag{8}$$

where $\boldsymbol{\lambda} > 0$, $k > 0$ are the parameters to be set, and the convergence speed of the system approaching stage can be adjusted by adjusting the parameters $\boldsymbol{\lambda}$ and k.

The control law can be obtained from (7) and (8):

$$\boldsymbol{u} = \boldsymbol{M}\left[\ddot{\boldsymbol{q}}_{\mathrm{d}} + \boldsymbol{c}\dot{\boldsymbol{e}} + \boldsymbol{\lambda}\text{sign}(\boldsymbol{s}) + k\boldsymbol{s}\right] + \boldsymbol{G} + \boldsymbol{C} - \boldsymbol{f}(t) \tag{9}$$

where $\boldsymbol{u} = \begin{cases} \boldsymbol{u}^+, & \boldsymbol{s} > 0 \\ \boldsymbol{u}^-, & \boldsymbol{s} < 0 \end{cases}$.

2.1. **Stability analysis.** Select the Lyapunov function:

$$V = \frac{1}{2}\boldsymbol{s}^2 \tag{10}$$

where $\boldsymbol{s}$ is the switching function.

Derivate both sides of (10) and introduce it into (7):

$$\dot{V} = \boldsymbol{s}\left(\left(\ddot{\boldsymbol{q}}_{\mathrm{d}} - \boldsymbol{M}^{-1}(\boldsymbol{u} + \boldsymbol{f}(t) - \boldsymbol{C} - \boldsymbol{G})\right) + \boldsymbol{c}\dot{\boldsymbol{e}}\right) \tag{11}$$

Substitute (9) into (11):

$$\dot{V} = \boldsymbol{s}\left(-\boldsymbol{c}\dot{\boldsymbol{e}} - \boldsymbol{\lambda}\text{sign}(\boldsymbol{s}) - k\boldsymbol{s} + \boldsymbol{c}\dot{\boldsymbol{e}}\right) = -k\boldsymbol{s}^2 - \boldsymbol{\lambda}\left|\boldsymbol{s}\right| < 0 \tag{12}$$

where $\text{sign}(\boldsymbol{s})$ is a signum function, $\text{sign}(\boldsymbol{s}) = \begin{cases} 1 & \boldsymbol{s} > 0 \\ 0 & \boldsymbol{s} = 0 \\ -1 & \boldsymbol{s} < 0 \end{cases}$.

According to the Lyapunov stability criterion, the system is asymptotically stable because of $V > 0$, $\dot{V} \leq 0$.

The theory analysis is verified based on a two-joint robotic manipulator.

$$\boldsymbol{M}(\boldsymbol{q}) = \begin{bmatrix} v + q_{01} + 2q_{02}\cos(q_2) & q_{01} + q_{02}\cos(q_2) \\ q_{01} + q_{02}\cos(q_2) & q_{01} \end{bmatrix},$$

$$\boldsymbol{C}(\boldsymbol{q}, \dot{\boldsymbol{q}}) = \begin{bmatrix} -q_{02}\dot{q}_2\sin(q_2) & -q_{02}(\dot{q}_1 + \dot{q}_2)\sin(q_2) \\ q_{02}\dot{q}_1\sin(q_2) & 0 \end{bmatrix},$$

$$\boldsymbol{G}(\boldsymbol{q}) = \begin{bmatrix} 15g\cos q_1 + 8.75g\cos(q_1 + q_2) \\ 8.75g\cos(q_1 + q_2) \end{bmatrix}, \ \boldsymbol{f}(t) = 3\sin(2\pi t)$$

For performance comparison, the traditional ILC controller and traditional SMC controller in [38] are also simulated under the same conditions. Select parameters of the controller as $v = 14$, $q_{01} = 8.98$, $q_{02} = 8.75$, $g = 9.8$.

Expected trajectories are: $q_{1\mathrm{d}} = \sin(3t)$, $q_{2\mathrm{d}} = \cos(3t)$.

Initial states are: $\boldsymbol{q}(0) = [0 \quad 1]^{\mathrm{T}}$, $\dot{\boldsymbol{q}}(0) = [3 \quad 0]^{\mathrm{T}}$.

Control parameters are: $c_1 = c_2 = 50$, $\lambda_1 = \lambda_2 = 0.5$, $k = 40$, set times of iterations to 10.

The system control block diagram is shown in Figure 1, where $u_k(t)$ and $u_{k+1}(t)$ are the signals of the previous control and the current control, $y_d(t)$ and $y_k(t)$ are the input signals and feedback signals, and $e_k(t)$ is the error.

Figure 2 shows the position tracking of 10 iterations and 10th iteration of ISMC. Figure 3 shows the position tracking of 10 iterations and 10th iteration of traditional ILC. Figure 4 shows the position tracking of traditional SMC. The control torque of ISMC and traditional SMC is shown in Figure 5. From Figure 2 to Figure 6, the following conclusions can be obtained.

1) Compared with traditional SMC and traditional ILC, ISMC can reduce the position tracking errors of the two joints of the robot arm with 0.0008 rad, 0.0019 rad and 0.0998 rad, 0.099 rad after the 10th iteration.

2) SMC can suppress chattering, and the control input signal generated by ISMC strategy is smoother than traditional SMC.

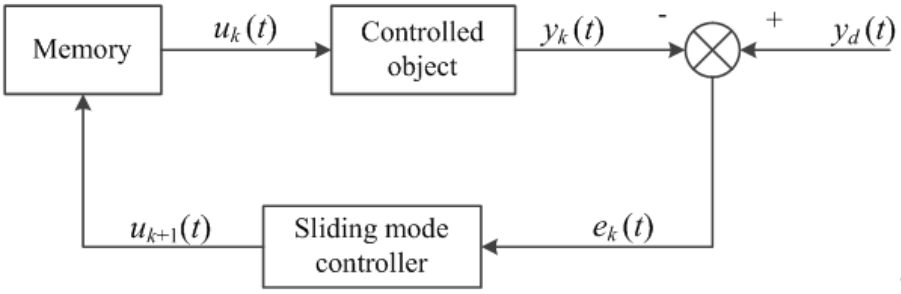

FIGURE 1. System control block diagram

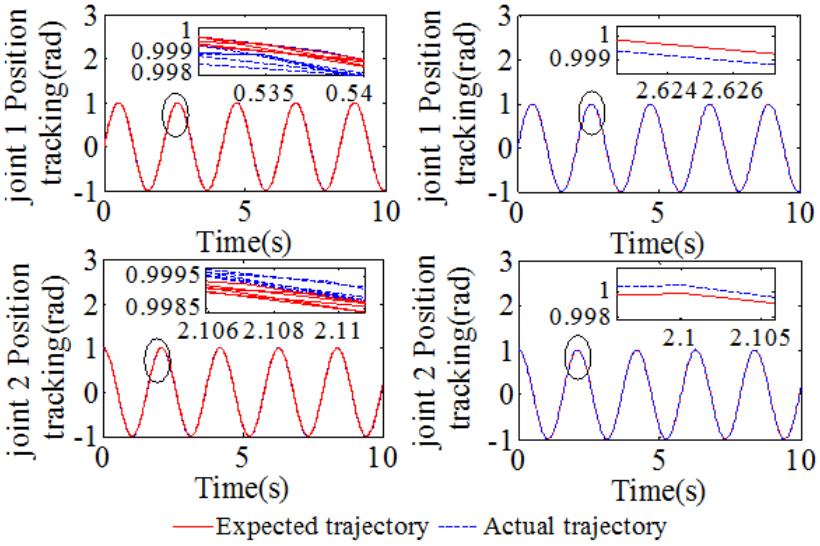

FIGURE 2. ISMC position tracking

In order to verify the robustness of iterative sliding mode control, a Gaussian disturbance function is introduced into the system: $f(t) = 1000\exp\left(-(t-3)^2/\left(2\times 0.1^2\right)\right)$. Among them, 1000 is the peak of the interference, 3 is the central time position of the interference, and 0.1 is the time domain degree of the interference.

Figure 6 shows the position tracking error curve under the ILC, SCM and ISMC strategy after the disturbance is introduced. It can be seen from Figure 6 that at the 3 s, a sudden change occurs in the position tracking error curve. In this process, it can be seen that the curve mutation degree is the largest under the ILC strategy, followed by the sudden change degree under the SMC strategy, and the curve is almost stable under the ISMC strategy. That is to say, the ILC has poor robustness, the SMC strategy enhances the anti-interference ability of the system, and the ISMC strategy makes the system more robust.

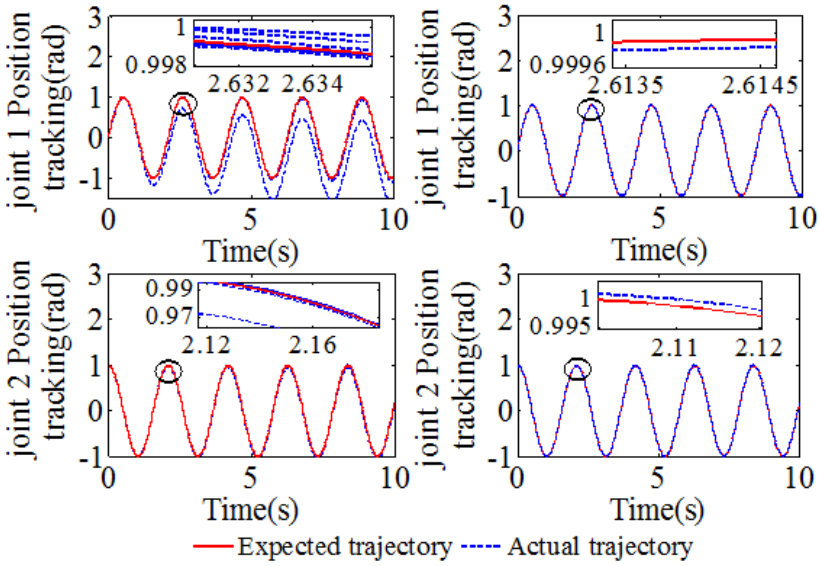

FIGURE 3. ILC position tracking

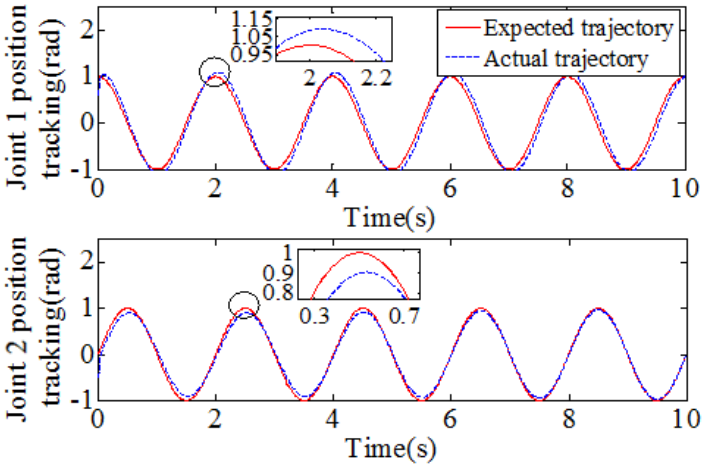

FIGURE 4. SMC position tracking

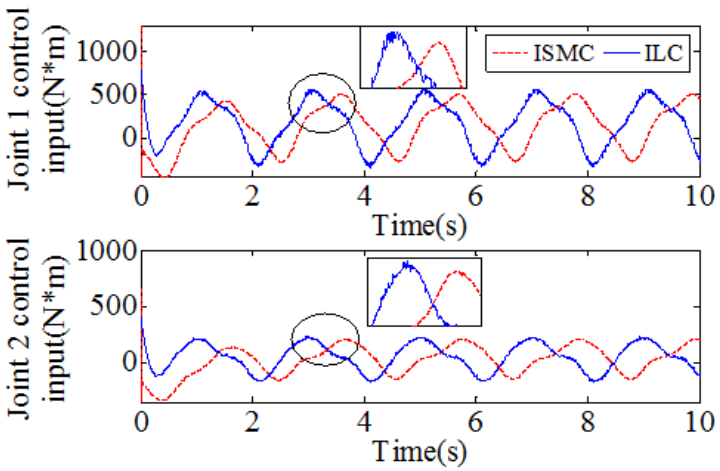

FIGURE 5. Control torque curve

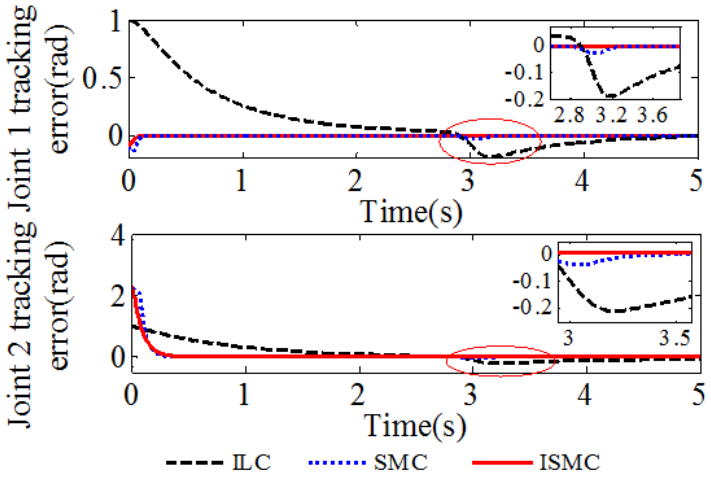

FIGURE 6. Position tracking error curve under interference

3. **Multi-Joint Synchronization Control Strategy.** The traditional synchronization error is defined as shown in the following formula:

$$\varepsilon_1 = e_1 - e_2, \ldots, \varepsilon_i = e_i - e_{i+1}, \varepsilon_n = e_n - e_1 \tag{13}$$

If the above-mentioned synchronization error definition form is used, there will be a cumulative effect of synchronization error between the joints of the mechanical arm. This cumulative effect will produce a phenomenon that the synchronization error becomes larger as the number of joints increases. The overall synchronization accuracy and performance of the robotic arm system have an adverse effect. Therefore, the paper introduces the concept of virtual main axis to improve the adverse effects caused by cumulative effect.

Assuming that there is an axis numbered 0 in the robot arm, the coordinate of the expected position given by the control is the same as that of the other joints, which is $q_{\mathrm{d}}(k)$, the state vector is $q_0(k)$, and the tracking error vector is $e_0(k)$. The synchronization error vector of each joint in the manipulator system is defined based on the assumed axis, that is $\varepsilon_i = [\varepsilon_i, \dot{\varepsilon}_i]^{\mathrm{T}}$, as shown in the following formula:

$$\varepsilon_i(k) = e_i(k-1) - e_0(k-1), \quad \varepsilon_i(1) = 0, \quad i = 1, 2, \ldots, n \tag{14}$$

By adopting this synchronization method, the cumulative error caused by the chain structure will not occur, and the synchronization motion accuracy of the robot arm system can be improved better. In the physical sense, the imaginary "0" axis does not exist, so it is defined as a virtual main axis, and its state vector $q_0(k)$ and tracking error $e_0(k)$ are defined by the average value as follows:

$$q_0(k) = \frac{1}{m}\sum_{i=1}^{m} q_i(k), \quad e_0(k) = \frac{1}{n}\sum_{i=1}^{n} e_i(k) = q_{\mathrm{d}}(k) - q_0(k) \tag{15}$$

Therefore, define the synchronization error as (16):

$$\varepsilon_1 = e_1 - e_0, \ldots, \varepsilon_i = e_i - e_0, \varepsilon_n = e_n - e_0 \tag{16}$$

Define the coupling error as (17):

$$\boldsymbol{E} = \boldsymbol{e} + \boldsymbol{a}\boldsymbol{\varepsilon} \tag{17}$$

where $\boldsymbol{e} = [e_1, \ldots, e_n]^{\mathrm{T}}$, $\boldsymbol{\varepsilon}_i(t) = [\varepsilon_1(t), \ldots, \varepsilon_n(t)]^{\mathrm{T}}$, $\boldsymbol{a}$ is a positive fixed matrix, which represents the control gain of the coupling error.

Compared with the cumulative effect of synchronization error brought by the traditional synchronization error definition method, the virtual spindle synchronization error definition method used in this article not only considers the position error of two adjacent joints, but also eliminates the mechanical error to a certain extent. The cumulative effect of the synchronization error between the various joints of the arm improves the body synchronization accuracy of the robotic arm system to a certain extent, and improves the adverse effects caused by the cumulative effect.

4. **Design of FOSMC Synchronization Controller.** A reasonable reaching law can greatly accelerate the approach speed and reduce system chattering. In this paper, a fractional order reaching law is designed using fractional calculus and SMC:

$$D^{\beta}s = -k\text{sign}(s) \tag{18}$$

where $0 < \beta < 1$, D is a calculus operator.

4.1. **Reaching law steady-state chatter analysis.** Take the traditional exponential approach law as an example:

$$\dot{s} = -\varepsilon\text{sign}(s) - ks \quad 0 < \varepsilon,\ k > 0 \tag{19}$$

When s approaches 0, its limit on the sliding surface is

$$\lim_{s\to 0}\dot{s} = \begin{cases} -\varepsilon & s \to 0^{+} \\ \varepsilon & s \to 0^{-} \end{cases} \tag{20}$$

It can be obtained from (19) that when s approaches 0, the system will chatter with amplitude e near the equilibrium point [39]. For the reaching law shown in (18) designed in this paper, when $s \to 0^{+}$ and $s \to 0^{-}$, there always $\dot{s} = 0$, which indicates that the system has no chattering phenomenon near the steady state.

4.2. **Reaching rate analysis.**

Proof: the approach rate of the fractional reaching law is greater than the exponential reaching law.

4.2.1. *The approach time of exponential reaching law.* It can be obtained from (19):

$$\dot{s} = -\varepsilon\text{sign}(s) - ks \tag{21}$$

When $s > 0$:

$$t_1' = \int_0^s \frac{\mathrm{d}s}{-\varepsilon\text{sign}(s) - ks} = \int_0^s \frac{\mathrm{d}s}{-\varepsilon - ks} = -\frac{1}{k}\left[\ln\left(1 + \frac{k}{\varepsilon}s\right)\right] \tag{22}$$

When $s < 0$:

$$t_2' = \int_0^{-s} \frac{\mathrm{d}s}{-\varepsilon\text{sign}(s) - ks} = \int_0^{-s} \frac{\mathrm{d}s}{\varepsilon - ks} = -\frac{1}{k}\left[\ln\left(1 + \frac{k}{\varepsilon}s\right)\right] \tag{23}$$

When $s = 0$, that is on the slip surface, $t_3' = 0$.

So the approach time of the exponential reaching law is

$$t' = \begin{cases} -\dfrac{1}{k}\left[\ln\left(1 + \dfrac{k}{\varepsilon}s\right)\right], & s \neq 0 \\ 0, & s = 0 \end{cases} \tag{24}$$

4.2.2. *The approach time of fractional order reaching law.* Since the derivative of Caputo does not satisfy the condition of semi-group, in order to solve this problem, we adopt the ∂ order Riemnnan-Liouvile fraction integral and obtain a standard derivative.

From the definition of Riemnnan-Liouvile fractional calculus, for a positive real number ∂, then the ath order Riemnnan-Liouvile fractional-order calculus of ∂ function $f(t)$ on the interval $[a, b]$ is defined as:

$$ {}_aD_t^{\partial} f(t) = \frac{1}{\Gamma(\partial)} \int_a^t (t-\tau)^{\partial-1} f(\tau) d\tau \tag{25} $$

Gamma function is defined as:

$$ \Gamma(\partial) = \int_a^{\infty} e^{-t} t^{z-1} dt \tag{26} $$

The following can be obtained from [40,41]:

$$ J^{\partial} D^{\partial} s = J^{\partial}(-k\text{sign}(s)),\ J^{\partial} f(t) = \frac{1}{\Gamma(\partial)} \int_0^t (t-\tau)^{\partial-1} f(\tau) d\tau \tag{27} $$

The simplified expression is $s(t) - s(0) = J^{\partial}(-k\text{sign}(s))$ applying a standard derivate:

$$ \dot{s} = -kDJ^{\partial}(-\text{sign}(s)) \tag{28} $$

For calculating the approach time:

$$ t^{\partial} = J^{\partial}\Gamma(1+\partial) \tag{29} $$

From (28) and (29):

$$ t^{\partial} dt = \frac{\Gamma(1+\partial)}{kD\text{sign}(s)} ds \to t^{\partial+1} = \frac{\Gamma(1+\partial)}{kD\text{sign}(s)(\partial+1)} ds \tag{30} $$

The approach time of the fractional order reaching law is

$$ \begin{cases} t = \sqrt[\partial+1]{\dfrac{\Gamma(1+\partial)s}{kD(\partial+1)}}, & s \neq 0 \\ 0, & s = 0 \end{cases} \tag{31} $$

It can be obtained from (24) and (31):

$$ \begin{cases} t' - t = \dfrac{\ln\left(1+\frac{k}{\varepsilon}s\right)}{-k} - \dfrac{\Gamma(1+\partial)s}{kD(\partial+1)} = \dfrac{\ln\left(\dfrac{\varepsilon \cdot e^{(-k)\cdot\partial+1\sqrt{\frac{\Gamma(1+\partial)s}{kD(\partial+1)}}}}{\varepsilon+ks}\right)}{k} > 0, & s \neq 0 \\ 0, & s = 0 \end{cases} \tag{32} $$

It can be obtained from the above derivation that the approach rate of the fractional reaching law is higher than the approach rate of the exponential reaching law.

4.3. **Stability analysis.** Use the Lyapunov function:

$$ V(t) = \frac{1}{2} s^{\mathrm{T}} s \tag{33} $$

According to the definition of Caputo-type fractional calculus:

$$ \begin{cases} \dot{s} > 0 \\ \dot{s} < 0 \end{cases} \Rightarrow \begin{cases} D^{\beta} s > 0 \\ D^{\beta} s < 0 \end{cases} \tag{34} $$

Take the derivative of (33), and the following can be obtained via (18) and (34):

$$\dot{V}(t) = s^{\mathrm{T}} s = s^{\mathrm{T}} D^{1-\beta}(-k\mathrm{sign}(s)) \tag{35}$$

Because of sign $\left(D^{1-\beta}(-k\mathrm{sign}(s))\right) = -k\mathrm{sign}(s)$ [42]:

$$\mathrm{sign}\left(\dot{V}(t)\right) = \mathrm{sign}\left(s^{\mathrm{T}}\right)\mathrm{sign}\left(D^{1-\beta}(-k\mathrm{sign}(s))\right) = -k\mathrm{sign}\left(s^{\mathrm{T}}\right)\mathrm{sign}(s) = -k \tag{36}$$

Then $\dot{V} \leq 0 \Rightarrow D^{\beta}V \leq 0$, selected fractional order reaching law is progressively stable.

4.4. **Design control law.** The design sliding surface is

$$\boldsymbol{s} = \boldsymbol{cE} + \dot{\boldsymbol{E}} \tag{37}$$

Fractional order reaching law is shown in (18).
Take the derivative of (18):

$$\dot{s} = D^{1-\beta}(-k)\mathrm{sign}(s) \tag{38}$$

Substitute (2), (4), and (17) into (37):

$$\dot{\boldsymbol{s}} = \boldsymbol{c}\dot{\boldsymbol{E}} + \boldsymbol{a}\ddot{\boldsymbol{\varepsilon}} + \ddot{\boldsymbol{q}}_{\boldsymbol{d}} - \boldsymbol{M}^{-1}\left[\boldsymbol{u} + \boldsymbol{f} - \boldsymbol{G} - \boldsymbol{C}\dot{\boldsymbol{q}}\right] \tag{39}$$

The control law can be obtained from (38) and (39):

$$\boldsymbol{u} = \boldsymbol{M}\left[\ddot{\boldsymbol{q}}_{\mathrm{d}} + \boldsymbol{c}\dot{\boldsymbol{E}} + \boldsymbol{a}\ddot{\boldsymbol{\varepsilon}} + kD^{1-\beta}\mathrm{sign}(s)\right] + \boldsymbol{G} + \boldsymbol{C}\dot{\boldsymbol{q}} - \boldsymbol{f} \tag{40}$$

Control law stability analysis, select the Lyapunov function:

$$V = \frac{1}{2}\boldsymbol{s}^2 \tag{41}$$

Take the derivative (41) and introduce (39) and (40):

$$\dot{V} = \boldsymbol{s}\dot{\boldsymbol{s}} = \boldsymbol{s}\left(\ddot{\boldsymbol{q}}_{\mathrm{d}} + \boldsymbol{c}\dot{\boldsymbol{E}} + \boldsymbol{a}\ddot{\boldsymbol{\varepsilon}} - \boldsymbol{M}^{-1}(\boldsymbol{u} + \boldsymbol{f} - \boldsymbol{C} - \boldsymbol{G})\right) = \boldsymbol{s}\left(-kD^{1-\beta}\mathrm{sign}(s)\right) \leq 0 \tag{42}$$

According to the Lyapunov stability criterion, the system is stable.

5. **Simulation Tests and Analysis.** The control block diagram of a cross-coupled synchronization is shown in Figure 7.

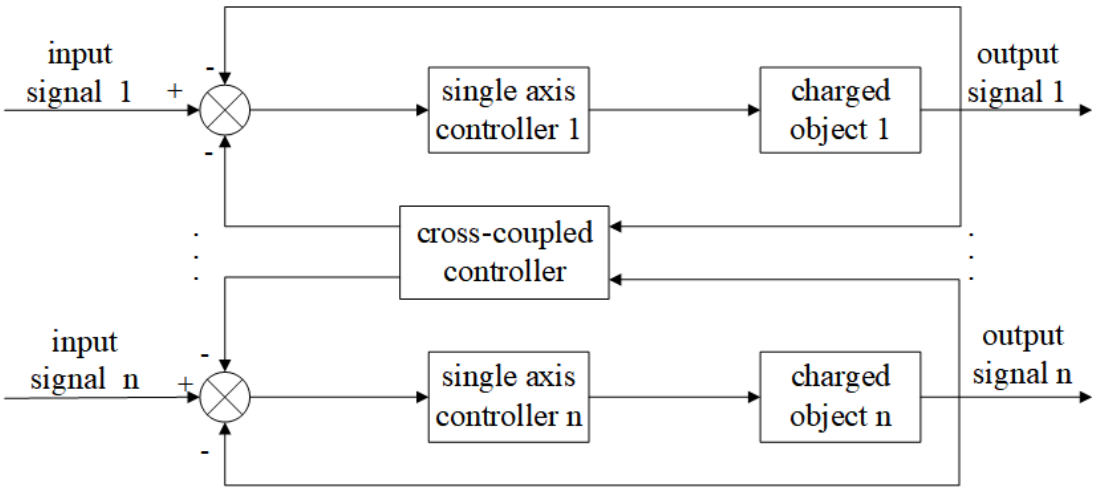

FIGURE 7. CCC block diagram

The simulation object is a three-joint industrial robot. According to the dynamic model derived above, the expressions of each matrix in the model are as follows:

$$\boldsymbol{C}(\boldsymbol{q},\dot{\boldsymbol{q}})=\begin{bmatrix} c_{11} & c_{12} & c_{13} \\ c_{21} & c_{22} & c_{23} \\ c_{31} & c_{32} & c_{33} \end{bmatrix},\ \boldsymbol{M}(\boldsymbol{q})=\begin{bmatrix} m_{11} & m_{12} & m_{13} \\ m_{21} & m_{22} & m_{23} \\ m_{31} & m_{32} & m_{33} \end{bmatrix}$$

$\boldsymbol{G}(\boldsymbol{q})=\begin{bmatrix} g_1 & g_2 & g_3 \end{bmatrix}^{\mathrm{T}}$, $\boldsymbol{q}=[q_1 \quad q_2 \quad q_3]^{\mathrm{T}}$

$m_{11}=I_1+a_1\cos^2(q_2)+a_2\cos^2(q_2+q_3)+2a_3\cos(q_2)\cos(q_2+q_3)$, $m_{33}=I_3+a_2$

$m_{12}=m_{21}=m_{13}=m_{31}=0$, $m_{22}=I_2+a_1+a_2+2a_3\cos(q_3)$

$m_{23}=m_{32}=a_2+a_3\cos(q_3)$

$$c_{11}=-\frac{1}{2}a_1\dot{q}_2\sin(2q_2)-\frac{1}{2}a_2\left(\dot{q}_2+\dot{q}_3\right)\sin(2q_2+2q_3)-a_3\dot{q}_2\sin(2q_2+q_3)$$
$$-a_3\dot{q}_3\cos(q_2)\sin(q_2+q_3)$$

$$c_{12}=-\frac{1}{2}a_1\dot{q}_1\sin(2q_2)-\frac{1}{2}a_2\dot{q}_1\sin(2q_2+2q_3)-a_3\dot{q}_1\sin(2q_2+q_3),\ c_{21}=-c_{12},\ c_{31}=-c_{13}$$

$$c_{33}=0,\ c_{13}=-\frac{1}{2}a_1\dot{q}_1\sin(2q_2+2q_3)-a_3\dot{q}_1\cos(q_2)\sin(q_2+q_3),\ c_{22}=-a_3\dot{q}_3\sin(q_3)$$

$c_{23}=-a_3(\dot{q}_2+\dot{q}_3)\sin(q_3)$, $c_{32}=-a_3\dot{q}_2\sin(q_3)$, $g_1=0$, $g_2=b_1\cos(q_2)+b_2\cos(q_2+q_3)$

$g_3=b_2\cos(q_2+q_3)$, $a_1=m_2r_2^2+m_3l_2^2$, $a_2=m_3l_3^2$, $a_3=m_3r_3l_2$, $m_2=30$ Kg, $m_3=26$ Kg

$b_1=(m_2r_2+m_3l_2)g$, $b_2=m_3r_3g$, $r_2=0.6$ m, $r_3=0.5$ m, $g=9.8$ m/s^2, $I_1=3.61$ Kg·m^2

$I_2=2.35$ Kg·m^2, $I_3=1.95$ Kg·m^2.

The paper compares the synchronous control strategy proposed in this paper with the traditional linear PD cross-coupling control (linear PD-CCC) strategy proposed in [42] and nonlinear PD ring coupling control (nonlinear PD-RCC) strategy proposed in [43].

In [43,44], scholars have designed a typical PD controller, which improves the synchronization control accuracy of the manipulator to a certain extent. However, the traditional linear PD-CCC controller proposed in [43] has a cumbersome process of proving the control law, many parameters need to be adjusted, and the control effect is not very ideal. The nonlinear PD-RCC controller proposed in [44] has a more complicated structure than the CCC controller, so the workload in the control process is larger, and the controller also has the problem that the parameters are not easy to adjust. Therefore, this paper proposes the FOSMC-CCC controller in response to the above problems. First, the ISMC position controller is designed to achieve accurate position tracking of each joint of the manipulator. Secondly, it avoids the difficulty of parameter adjustment in traditional PD control, its controller design is simple, and the introduction of fractional calculus theory further improves the control accuracy of the system.

The linear PD-CCC is: $\boldsymbol{u}=\boldsymbol{K_P}\boldsymbol{E}+\boldsymbol{K_D}\dot{\boldsymbol{E}}+(\boldsymbol{I}+\boldsymbol{aT})^{-1}\boldsymbol{K_e}\dot{\boldsymbol{e}}$.

Parameters are set to: $\boldsymbol{K_P}=\mathrm{diag}(25)$, $\boldsymbol{K_D}=\mathrm{diag}(10)$, $\boldsymbol{K_e}=\mathrm{diag}(20)$, $\boldsymbol{a}=[0.3 \quad 0.3 \quad 0.3]$.

The nonlinear PD-RCC is: $\boldsymbol{u}=\boldsymbol{K_P}\tanh(\boldsymbol{e})+\boldsymbol{K_D}\dot{\boldsymbol{e}}+\boldsymbol{K_e}\boldsymbol{E}$, where $\tanh(\cdot)$ is the hyperbolic tangent function.

Parameters are set as follows: $\boldsymbol{K_P}=\mathrm{diag}(25)$, $\boldsymbol{K_D}=\mathrm{diag}(10)$, $\boldsymbol{K_e}=\mathrm{diag}(20)$.

The FOSMC-CCC with virtual spindle designed in this paper uses MATLAB/FOMCON toolbox to complete the numerical simulation [45].

Parameters are set as follows: $\mathrm{diag}(c_1,c_2,c_3)=\mathrm{diag}(50,50,50)$, $\boldsymbol{a}=[0.3 \quad 0.3 \quad 0.3]$.

When the input signal is a step response, the position tracking error curve of the robot arm joint under different synchronization error definitions is shown in Figure 8. It can

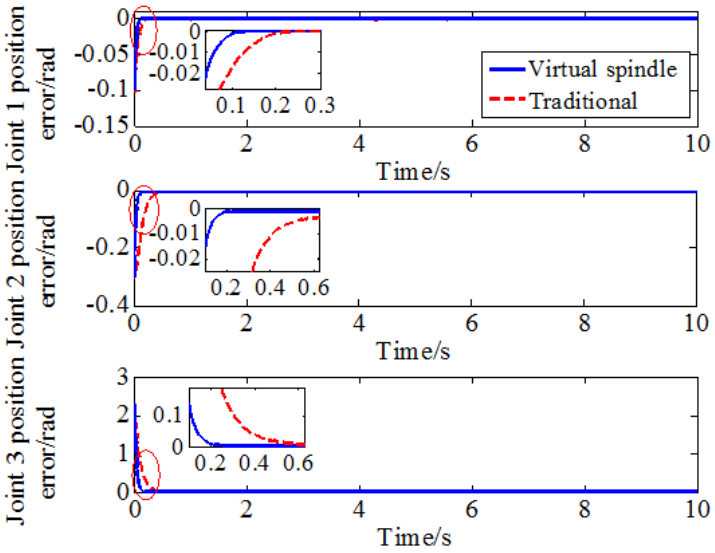

FIGURE 8. Position tracking error curve under different synchronization errors

be seen from Figure 8 that compared with traditional definition of synchronization error, after introduction of the virtual spindle in the synchronization error, tracking error of each joint of the robot arm are smaller, tracking effect is better, and control accuracy is higher.

It can be seen from (18) that the value of β affects the approach speed of the fractional approach law, which in turn affects the control accuracy and control effect of the control system. Therefore, it is very important to choose an appropriate β value. The following will discuss the fetching of β from the position error norm convergence situation and the speed error norm convergence situation.

Figure 9 shows the convergence process of maximum absolute value of the position error norm under different β values. Figure 10 shows the convergence process of the maximum absolute value of the speed error norm under different β values. As can be seen from Figure 9 and Figure 10, it is most appropriate when the value of β is approximately 0.2. Because when $\beta > 0.2$, the speed error norms of the three joints of manipulator are divergent and not convergent. And when $\beta = 0.2$, the maximum and minimum values of position error norm and the maximum and minimum values of speed error norm of the

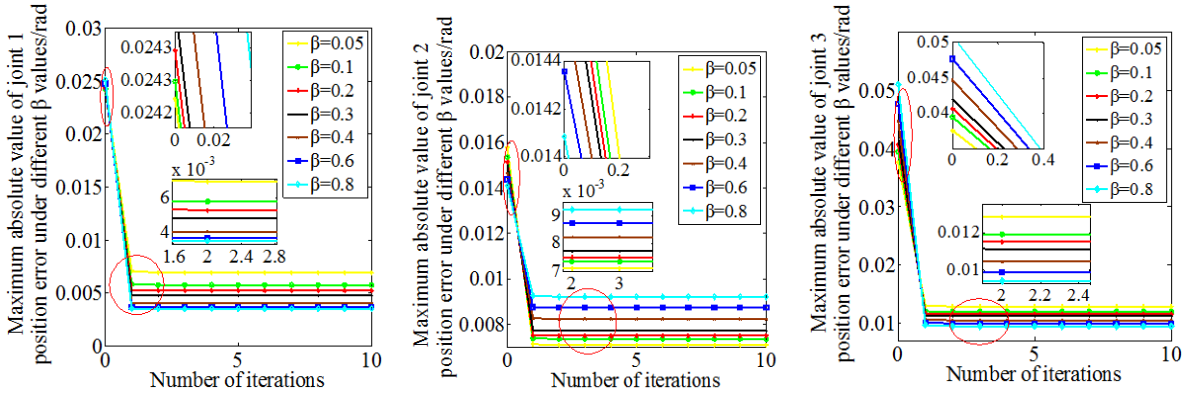

(a) Joint 1 error norm (b) Joint 2 error norm (c) Joint 3 error norm

FIGURE 9. Convergence process of position error norm under different β values

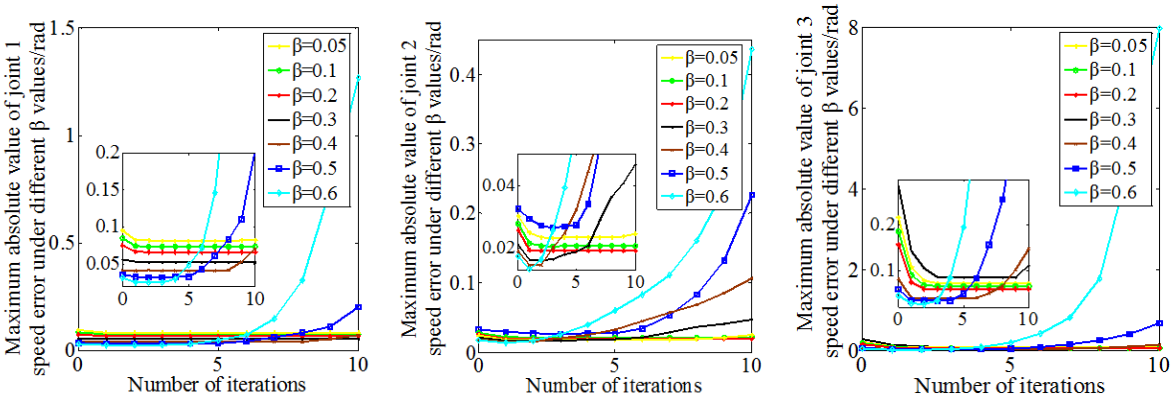

(a) Joint 1 error norm (b) Joint 2 error norm (c) Joint 3 error norm

FIGURE 10. Convergence process of speed error norm under different β values

three joints of robot arm are the most suitable. So set the fractional order $\beta = 0.2$ of FOSMC-CCC.

When the desired trajectory is given as a step signal, the initial state is:

$$\boldsymbol{q}(0) = [0.6 \quad 0.8 \quad -1.8]^{\mathrm{T}}, \quad \dot{\boldsymbol{q}}(0) = [0 \quad 0 \quad 0]^{\mathrm{T}}$$

The disturbance is: $f(t) = 1000 \exp\left(-(t-3)^2/\left(2 \times 0.1^2\right)\right)$.

Figure 11 shows the position tracking curve of the three-joint manipulator by three synchronous control strategies, and the step response performance index is shown in Table 1. From Figure 11 and Table 1, it can be obtained that when the synchronous controller is a fractional sliding mode controller, the dynamic performance indicators and steady-state performance indicators in the unit step response can be satisfied better.

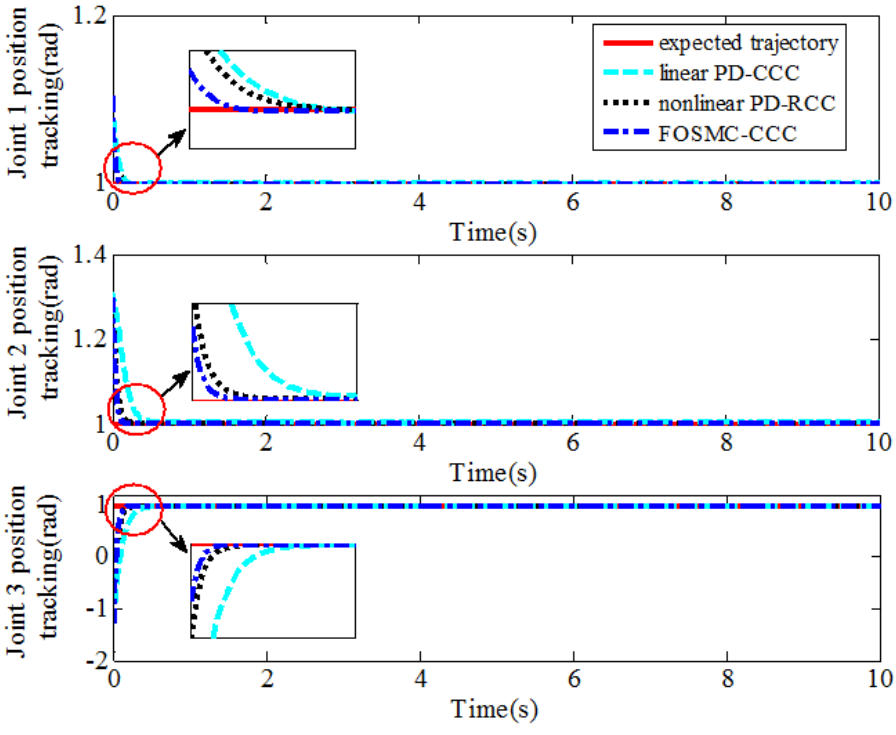

FIGURE 11. Position tracking curve

TABLE 1. Unit step response performance indicators

		Overshoot (%)	Adjust the time (s)	Steady-state error (rad)
Linear PD-CCC	Joint 1	0.08	0.27	< 0.0006
	Joint 2	0	0.64	< 0.0003
	Joint 3	0	0.61	< 0.0008
Nonlinear PD-RCC	Joint 1	0.07	0.25	< 0.0005
	Joint 2	0	0.42	< 0.0002
	Joint 3	0	0.37	< 0.0006
FOSMC-CCC	Joint 1	0.05	0.13	< 0.0004
	Joint 2	0	0.22	< 0.0001
	Joint 3	0	0.26	< 0.0005

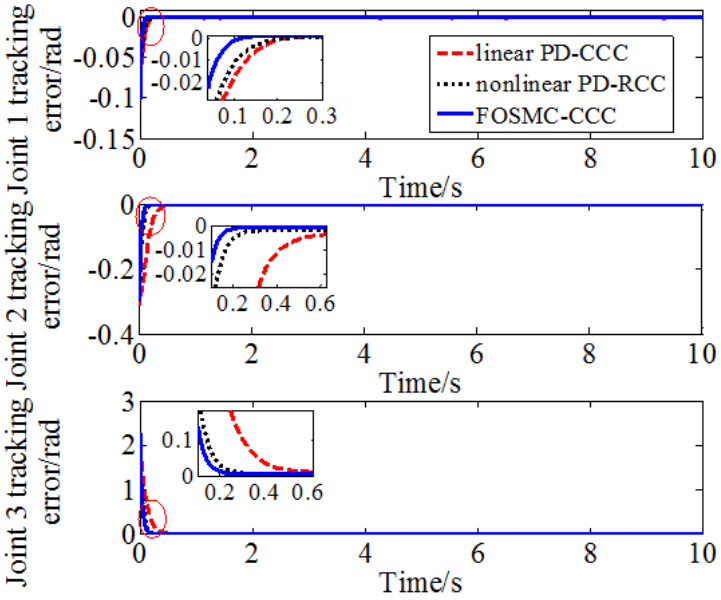

FIGURE 12. Position tracking error

Figure 12 and Figure 13 show the tracking error curve, the synchronization error curve, and coupling error curve, respectively. Table 2 shows the comparison of data. Take the angular displacement adjustment time, the RMSE of the position error, the RMSE of the synchronization error, and the RMSE of the coupling error as reference values. It is available from Figure 12, Figure 13 and Table 2:

1) Compared with linear PD-CCC, the RMSE of the position error of FOSMC-CCC is reduced by 0.0024 rad, 0.0178 rad and 0.0124 rad, and compared with non-linear PD-RCC by 0.001 rad, 0.0029 rad and 0.0029 rad.

2) Compared with linear PD-CCC, the RMSE of the synchronization error of FOSMC-CCC is reduced by 0.0103 rad, 0.0094 rad and 0.0834 rad, and compared with non-linear PD-RCC by 0.006 rad, 0.0043 rad and 0.0102 rad.

3) Compared with linear PD-CCC, the angular displacement adjustment time of FOSMC-CCC is reduced by 0.13 s, 0.43 s and 0.44 s, and compared with non-linear PD-RCC, it is reduced by 0.1 s, 0.13 s and 0.17 s. Therefore, the accuracy of manipulator system is higher and operation of each joint is more stable and reliable when FOSMC-CCC is used.

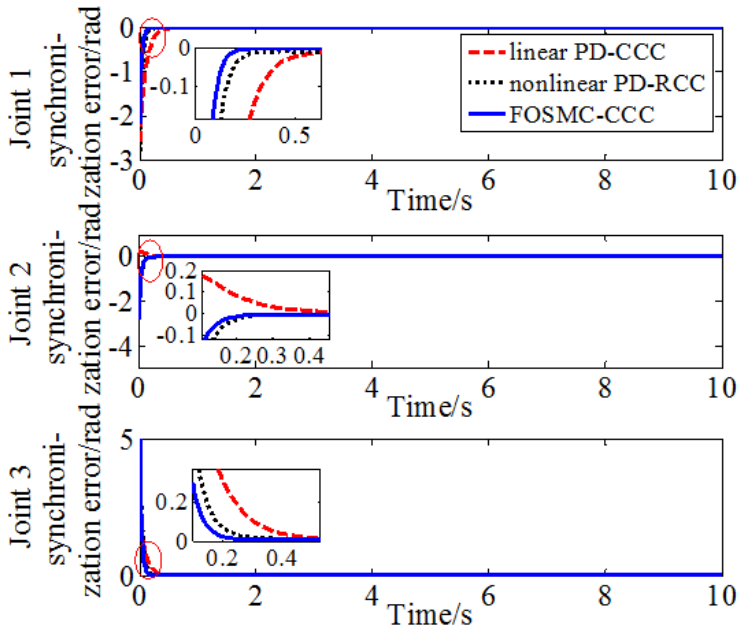

FIGURE 13. Position synchronization error

TABLE 2. Data comparison of robot arm joints

	Linear PD-CCC	Nonlinear PD-RCC	FOSMC-CCC
Joint 1 angular displacement adjustment time (s)	0.28	0.25	0.15
Joint 2 angular displacement adjustment time (s)	0.62	0.32	0.19
Joint 3 angular displacement adjustment time (s)	0.68	0.41	0.24
RMSE of position error of Joint 1 after 2 s (rad)	0.0036	0.0022	0.0012
RMSE of position error of Joint 2 after 2 s (rad)	0.0554	0.0405	0.0376
RMSE of position error of Joint 3 after 2 s (rad)	0.0878	0.0783	0.0754
RMSE of synchronization error of Joint 1	0.0552	0.0509	0.0449
RMSE of synchronization error of Joint 2	0.1047	0.0996	0.0953
RMSE of synchronization error of Joint 3	0.1889	0.1157	0.1055

In order to further verify the system performance, the sinusoidal signals are used as the desired trajectories, which are as shown below:

$$\begin{cases} q_{1\mathrm{d}} = 1.1 + 1.2\sin(\pi t),\ q_{2\mathrm{d}} = 0.1 + 1.2\cos(\pi t),\ q_{3\mathrm{d}} = -1.3 + 1.2\sin(\pi t) \\ \dot{q}_{1\mathrm{d}} = 1.2\pi\cos(\pi t),\ \dot{q}_{2\mathrm{d}} = -1.2\pi\sin(\pi t),\ \dot{q}_{3\mathrm{d}} = 1.2\pi\cos(\pi t) \end{cases}$$

The initial state is: $q(0) = [1.1 \quad 1.3 \quad -1.3]^{\mathrm{T}}$, $\dot{q}(0) = [1.2\pi \quad 0 \quad 1.2\pi]^{\mathrm{T}}$.

Set the times of iteration is 10. The following results can be obtained based on the experiments performed on MATLAB.

Figure 14 shows the output torque of the coupled controller under the three synchronous control strategies. It can be concluded that the output torque of the coupled controller of the linear PD-CCC is the largest, where the Joint 2 is close to 500 N·m. The output torque of the coupled controller of nonlinear PD-RCC is the second, where the Joint 2 is close to 400 N·m. The output torque of the FOSMC-RCC coupling controller is the smallest, and the torque of the Joint 1 is the largest, which is close to 50 N·m. And the coupled controller under nonlinear PD-RCC has local chattering.

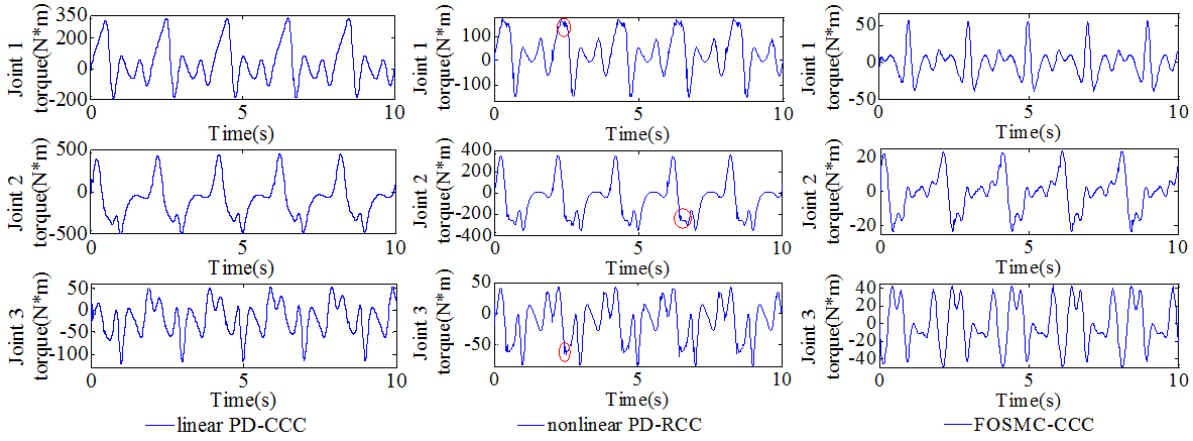

FIGURE 14. Coupling output torque under different synchronous control strategies

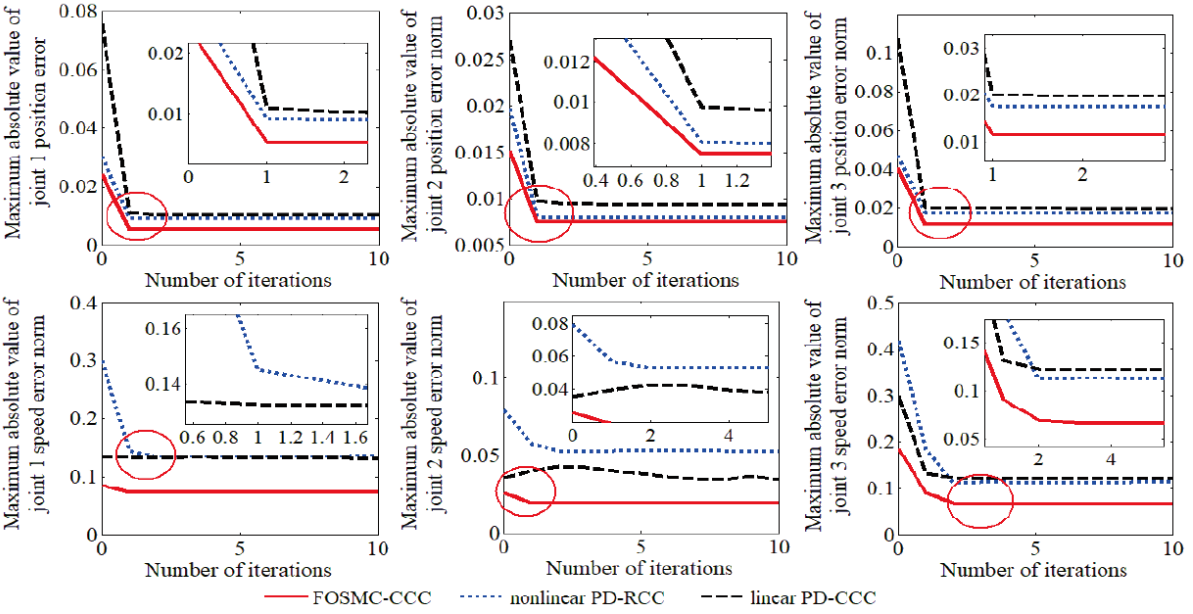

FIGURE 15. Position (velocity) error norm convergence process

Figure 15 shows the maximum absolute value convergence curve of the position errors of three joints for the robotic manipulator after 10 iterations under the three synchronous control strategies. The comparison can be concluded as follows.

In linear PD-CCC, the maximum absolute values of the position errors of the three joints are 0.0758, 0.0270 and 0.1076, and the minimum absolute values are 0.0101, 0.0093 and 0.0196. The maximum absolute values of the speed errors of the three joints are 0.1352, 0.0428 and 0.2981, and the minimum absolute values are 0.1321, 0.0350 and 0.1226.

In nonlinear PD-RCC, the maximum absolute values of the position errors of the three joints are 0.0305, 0.0197 and 0.0473, and the minimum absolute values are 0.0090, 0.0079 and 0.0174. The maximum absolute values of the speed errors of the three joints are 0.3002, 0.0795 and 0.4181, and the minimum absolute values are 0.1351, 0.0529 and 0.1120.

In FOSMC-CCC, the maximum absolute values of the position errors of the three joints are 0.0243, 0.0160 and 0.0370, and the minimum absolute values are 0.0072, 0.0065 and

0.0133. The maximum absolute values of the speed errors of the three joints are 0.1491, 0.0477 and 0.3323, and the minimum absolute values are 0.1065, 0.0341 and 0.0921.

As a whole, the maximum absolute value of the position error norm and the maximum absolute value of the speed error norm of the FOSMC-CCC strategy are the smallest. Therefore, compared with the traditional linear PD-CCC control strategy and nonlinear PD-RCC control strategy, under the FOSMC-CCC control strategy, the position tracking control accuracy of the robot arm control system is higher, the synchronization performance between joints is better, and the contour error of the system is smaller.

6. **Conclusions.** In order to improve the accuracy of the control for the robotic manipulator, the control strategies of a single joint position tracking control strategy based on ISMC and a multi-joint cross-coupling control strategy based on PD control, SMC control, and FOSMC control are proposed. The following conclusions are obtained.

1) The ISMC strategy based on the idea of combining ILC and SMC is proposed to improve the tracking speed and tracking accuracy of a single joint. Take position tracking, input of the control, and convergence of the maximum absolute value of position error as the basis for judgment. Compared with traditional SMC strategy and traditional ILC strategy, ISMC has better tracking effect, stronger robustness, but less system chatter.

2) Three different CCC strategies are designed respectively. Take dynamic performance index, steady-state performance index, angular displacement adjustment time, and RMSE as main performance indicators. The results show that the dynamic performance index and steady-state performance index of FOSMC-CCC strategy is better than linear PD-CCC and nonlinear PD-RCC strategy, and the angular displacement adjustment time and RMSE are smaller, which meets the synchronization accuracy.

3) As for future work, the aim is to introduce the friction term in the actual model to make it closer to the actual situation. And it is extended to the fields of n-joint manipulator control, synchronous motor control, spacecraft attitude tracking, etc., and tested through experiments.

Acknowledgment. This work is partially supported by the National Natural Science Foundation of China (No. 61663022), Gansu Provincial Department of Education Project (No. 18JR3RA105). The authors also gratefully acknowledge the helpful comments and suggestions of the reviewers, which have improved the presentation.

REFERENCES

[1] C. Xiao, Y. L. Zhou, H. Y. Sheng and Y. L. Hou, Modular design of mechanical noumenon for industrial robots, *China Mechanical Engineering*, vol.27, no.8, pp.1018-1025, 2016.

[2] Q. V. Doan, T. D. Le and A. T. Vo, Synchronization full-order terminal sliding mode control for an uncertain 3-DOF planar parallel robotic manipulator, *Applied Sciences*, vol.9, no.9, pp.1-17, 2019.

[3] L. Han, H. Hu, W. H. Ding and J. J. Li, Tension control methodology of active continuous discharge and intermittent reciprocating work based on master-slave synchronous motion, *International Conference on Civil, Architecture and Environmental Engineering*, vol.1, pp.781-786, 2017.

[4] S. M. Park, H. W. Kim, H. J. Kim and J. Y. Choi, Accuracy improvement of master-slave synchronization in EtherCAT networks, *IEEE Access*, vol.8, pp.58620-58628, 2020.

[5] Z. L. Huang, G. Q. Song, Y. M. Li and M. N. Sun, Synchronous control of two counter-rotating eccentric rotors in nonlinear coupling vibration system, *Mechanical Systems and Signal Processing*, vol.114, no.1, pp.68-83, 2019.

[6] K. Lee, J. I. Ha and D. V. Simili, Analysis and suppression of slotting and cross-coupling effects on current control in PM synchronous motor drives, *IEEE Trans. Power Electronics*, vol.34, no.10, pp.9942-9956, 2019.

[7] Z. L. Huang, Y. M. Li, G. Q. Song, X. L. Zhang and Z. C. Zhang, Speed and phase adjacent cross-coupling synchronous control of multi-exciters in vibration system considering material influence, *IEEE Access*, vol.7, pp.63204-63216, 2019.

[8] J. He, L. Mi, J. H. Liu, X. Cheng, Z Z. Lin and C. F. Zhang, Ring coupling-based collaborative fault-tolerant control for multi-robot actuator fault, *International Journal of Robotics and Automation*, vol.33, no.6, pp.672-680, 2018.
[9] Y. Koren, Cross-coupled biaxial computer controls for manufacturing systems, *Journal of Dynamic Systems Measurement & Control*, vol.102, no.4, pp.265-272, 1980.
[10] G. Zhong, Z. Shao, H. Deng and J. L. Ren, Precise position synchronous control for multi-axis servo systems, *IEEE Trans. Industrial Electronics*, vol.64, no.5, pp.3707-3717, 2017.
[11] S. Y. Hu, S. Qian, W. Wu and Q. Li, Position synchronization control for linear switch reluctance motor based on adjacent cross-coupling, *Proc. of the CSEE*, vol.37, no.23, pp.7024-7031, 2017.
[12] W. Budiharto, E. Irwansyah, J. S. Suroso and A. A. S. Gunawan, Design of object tracking for military robot using PID controller and computer vision, *ICIC Express Letters*, vol.14, no.3, pp.289-294, 2020.
[13] A. Boulkroune and A. Bouzeriba, Fuzzy generalized projective synchronization of incommensurate fractional-order chaotic systems, *Neurcomputing*, vol.173, pp.606-614, 2016.
[14] R. Ortega and M. W. Spong, Adaptive motion control of rigid robot: A tutorial, *Automatica*, vol.25, no.6, pp.877-888, 1989.
[15] Z. H. Man, A. P. Paplinski and H. R. Wu, A robust MIMO terminal sliding mode control scheme for rigid robotic manipulators, *IEEE Trans. Automatic Control*, vol.39, no.12, pp.2464-2469, 1994.
[16] A. Riani, T. Madani, A. Benallegue and K. Djouanib, Adaptive integral terminal sliding mode control for upper-limb rehabilitation exoskeleton, *Control Engineering Practice*, vol.75, pp.108-117, 2018.
[17] D. Matouk, F. Abdessemed, O. Gherouat and Y. Terchi, Second-order sliding mode for position and attitude tracking control of quadcopter UAV: Super-twisting algorithm, *International Journal of Innovative Computing, Information and Control*, vol.16, no.1, pp.29-43, 2020.
[18] Y. Byungyong, Normalized learning rule for iterative learning control, *International Journal of Control Automation & Systems*, vol.16, no.3, pp.1379-1389, 2018.
[19] Q. Y. Yang, Q. Z. Yan, J. P. Cai, J. H. Tian and X. H. Guan, Neural network-based error-tracking iterative learning control for tank gun control systems with arbitrary initial states, *IEEE Access*, vol.8, pp.72179-72187, 2020.
[20] L. L. Yang, J. Wang, F. Wang and W. M. Shi, Research on vibration suppression of linear servo system based on optimal control iterative learning, *Journal of Mechanical Engineering*, vol.55, no.15, pp.217-225, 2019.
[21] R. H. Chi, Z. S. Hou and B. Huang, Optimal iterative learning control of batch processes: From model-based to data-driven, *Acta Automatica Sinica*, vol.43, no.6, pp.917-932, 2017.
[22] W. Xu and F. Zhang, Learning Pugachev's cobra maneuver for tail-sitter UAVs using acceleration model, *IEEE Robotics and Automation Letters*, vol.5, no.2, pp.3452-3459, 2020.
[23] W. L. Li, X. H. Shi, X. H. Zou, D. Guo, Y. Yu and P. Yi, A dynamic road load simulation system for vehicle drivetrains, *Journal of Vibration and Shock*, vol.35, no.5, pp.163-167, 2016.
[24] D. M. Huang, L. J. Han, G. Y. Tang, Z. C. Zhou and G. H. Xu, Fractional integral sliding mode control for trajectory tracking of underwater manipulators, *China Mechanical Engineering*, vol.30, no.13, pp.1513-1518, 2019.
[25] S. Han, W. C. Cheng and D. F. Bao, Sliding mode control for ball screw drives based on variable power reaching law, *Journal of Southeast University (Natural Science Edition)*, vol.49, no.2, pp.237-244, 2019.
[26] M. Ye and H. Wang, A robust adaptive chattering-free sliding mode control strategy for automotive electronic throttle system via genetic algorithm, *IEEE Access*, vol.8, pp.68-80, 2020.
[27] M. Torabi, M. Sharifi and G. Vossoughi, Robust adaptive sliding mode admittance control of exoskeleton rehabilitation robots, vol.25, no.5, pp.2628-2642, 2018.
[28] C. Y. Tan and J. Wang, Robust iterative learning control based on extended state observer, *Control Theory & Applications*, vol.35, no.11, pp.1680-1686, 2018.
[29] S. Zaare and M. R. Soltanpour and M. Moattari, Voltage based sliding mode control of flexible joint robot manipulators in presence of uncertainties, *Robotics and Autonomous Systems*, vol.118, pp.204-219, 2019.
[30] X. M. Zhao and H. Y. Jin, Segmented variable universe fuzzy iterative learning control for permanent magnet linear synchronous motor servo system, *Transactions of China Electrotechnical Society*, vol.32, no.23, pp.9-15, 2017.
[31] C. M. Zheng, J. S. Zheng and R. Chen, Discrete-time sliding mode control based on improved disturbance compensation reaching law, *Control and Decision*, vol.34, no.4, pp.880-884, 2019.

[32] W. L. Li, X. H. Shi, J. Ke, B. Deng, Q. Shi, X. H. Zou and J. J. Wang, Engine torque pulsation simulation under idling speed based on sliding mode and iterative learning control, *Journal of Vibration, Measurement & Diagnosis*, vol.36, no.2, pp.359-365, 2016.

[33] Z. Z. Zhang, D. Ye and Z. W. Sun, Sliding mode fault tolerant attitude control for satellite based on iterative learning observer, *Journal of National University of Defense Technology*, vol.40, no.1, pp.17-23, 2018.

[34] C. Yin, Y. Cheng, S. M. Zhong and J. W. Cao, Fractional-order sliding mode-extremum seeking control design with fractional-order PI sliding surface, *Proc. of the 34th China Control Conference*, 2015.

[35] K.-J. Zhang, G.-H. Peng and J.-J. Dou, Robustness of PD$\sim\alpha$ type iterative learning control for fractional-order linear time-delay systems, *Science Technology and Engineering*, vol.18, no.20, pp.130-134, 2018.

[36] S. M. Song, L. W. Deng and X. L. Chen, Application characteristics of fractional calculus in sliding mode control, *Journal of Chinese Inertial Technology*, vol.22, no.4, pp.439-444, 2014.

[37] H. Delavari, D. Baleanu and J. Sadati, Stability analysis of Caputo fractional-order nonlinear systems revisited, *Nonlinear Dynamics*, vol.67, no.4, pp.2433-2439, 2012.

[38] J. K. Liu, *Design of Robot Control System and MATLAB Simulation*, Tsinghua University Publishers, Peking, 2008.

[39] Y. Tian and Y. L. Cai, A new variable power reaching law for sliding mode control, *Journal of Chinese Inertial Technology*, vol.2, pp.241-247, 2019.

[40] S. Umarov, *Introduction to Fractional and Pseudo-Differential Equations with Singular Symbols*, Springer Publishers, New Haven, 2015.

[41] F. M. Benito, R. Rolando, T. Anthony and F. Carlos, *Application of Fractional Calculus to Oil Industry*, Intech Publishers, London, 2017.

[42] Y. Li, Y. Q. Chen and I. Podlubny, Technical communique: Mittag-Leffler stability of fractional order nonlinear dynamic systems, *Automatica*, vol.45, no.8, pp.1965-1969, 2009.

[43] S. H. Yu and X. H. Yu, Continuous finite-time control for robotic manipulators with terminal sliding mode, *Automatica*, vol.41, no.11, pp.1957-1964, 2005.

[44] K. P. Liu, Y. Qin and H. T. Yang, Nonlinear ring coupling compensation synchronization control for multi-axis industrial robot, *Mechanical Science and Technology for Aerospace Engineering*, vol.37, no.6, pp.910-914, 2018.

[45] A. Tepljakov, E. Petlenkov and J. Belikov, FOMCON: Fractional-order modeling and control toolbox for MATLAB, *IEEE Proc. of 2011 International Conference Mixed Design of Integrated Circuits and Systems-Mixdes*, pp.684-689, 2011.